Methods 206 (2022) 87–98

Contents lists available at ScienceDirect

Methods

journal homepage: www.elsevier.com/locate/ymeth

Advances in the exact nuclear Overhauser effect 2018–2022

Alya Hussain [a], Natasia Paukovich [a], Morkos A. Henen [a,b], Beat Vögeli [a,*]

[a] Department of Biochemistry & Molecular Genetics, School of Medicine, University of Colorado, 12801 E. 17th Avenue, Aurora, CO 80045, USA
[b] Department of Pharmaceutical Organic Chemistry, Faculty of Pharmacy, Mansoura University, Mansoura 35516, Egypt

ARTICLE INFO

Keywords:
Exact NOE
eNOE
Nuclear Overhauser Effect
Nuclear Magnetic Resonance

ABSTRACT

The introduction of the exact nuclear Overhauser enhancement (eNOE) methodology to solution-state nuclear magnetic resonance (NMR) spectroscopy results in tighter distance restraints from NOEs than in convention analysis. These improved restraints allow for higher resolution in structure calculation and even the disentanglement of different conformations of macromolecules. While initial work primarily focused on technical development of the eNOE, structural studies aimed at the elucidation of spatial sampling in proteins and nucleic acids were published in parallel prior to 2018. The period of 2018–2022 saw a continued series of technical innovation, but also major applications addressing biological questions. Here, we review both aspects, covering topics from the implementation of non-uniform sampling of NOESY buildups, novel pulse sequences, adaption of the eNOE to solid-state NMR, advances in eNOE data analysis, and innovations in structural ensemble calculation, to applications to protein, RNA, and DNA structure elucidation.

1. Introduction

The implementation of the Nuclear Overhauser Effect or Enhancement (NOE) to study biological molecules revolutionized our understanding of molecular structures [1]. The NOE, initially applied to uncover the structural elements of small molecules [2–5], evolved in the 1970s to characterize molecular distances and ligand-binding [4,6,7].

NMR methods to detect biomolecular motion advanced in parallel. Now widely appreciated to sample conformations over a range of timescales [8,9], dynamic biomolecular conformations may go undetected by X-ray crystallography and cryo-EM [10].

[10]. Indeed, the seminal X-ray crystal structure of the oxygen storage protein myoglobin in 1958 [11] was followed by recognition that the mechanism of the heme prosthetic group binding and unbinding oxygen is occluded in the static depiction [12,13]. NMR, however, is particularly suited to assess both the structure and dynamics of biomolecules tumbling freely and at near-physiologic conditions [14,15]. The detection of dynamics in globular proteins by NMR as a complement to X-ray crystal structures [16–18] began with the characterization of aromatic ring flips [19–21], and evolved to capture secondary and tertiary structural dynamics on a range of timescales [8,9].

The mid-1980 s to 1990 s saw the elucidation of protein structures relying on semi-quantitative NOE-derived distance restraints [22], first using the 2D homonuclear NOE Spectroscopy (NOESY) [23–25]and subsequently 3D and 4D NOESY [26,27].

From there, NOE advancements continued to narrow the gap between the characterization of structure and dynamics. First attempts to interpret NOEs using multiple conformations were reported for a β-hairpin forming linear peptide in the mid- to late-1990 s [28]. Conventional NOEs typically convey a single structure, representing an average of the multiple states or conformations a molecule occupies. The advent of the exact NOE (eNOE), a quantitative approach to the NOE, significantly improves structural resolution and multi-state structure calculations, adding to the repertoire of NMR experiments capturing biomolecular structure and dynamics. The most recent eNOE review covered advancements into 2018 and focused on the elucidation of large protein and RNA conformational ensembles via eNOE measurements [29]. Here, we summarize eNOE theory and explain the advantages of the eNOE over the conventional NOE in structure calculation in Section 2. We then summarize recent technical advances, reviewing topics from the implementation of non-uniform sampling and novel pulse sequences, adaption to solid-state NMR, and innovations in data analysis and structural ensemble calculation in Section 3. Biological applications to nucleic acid and protein structure elucidation are discussed in Section 4.

* Corresponding author.
E-mail address: beat.vogeli@cuanschutz.edu (B. Vögeli).

https://doi.org/10.1016/j.ymeth.2022.08.006
Received 21 May 2022; Received in revised form 5 August 2022; Accepted 12 August 2022
Available online 17 August 2022

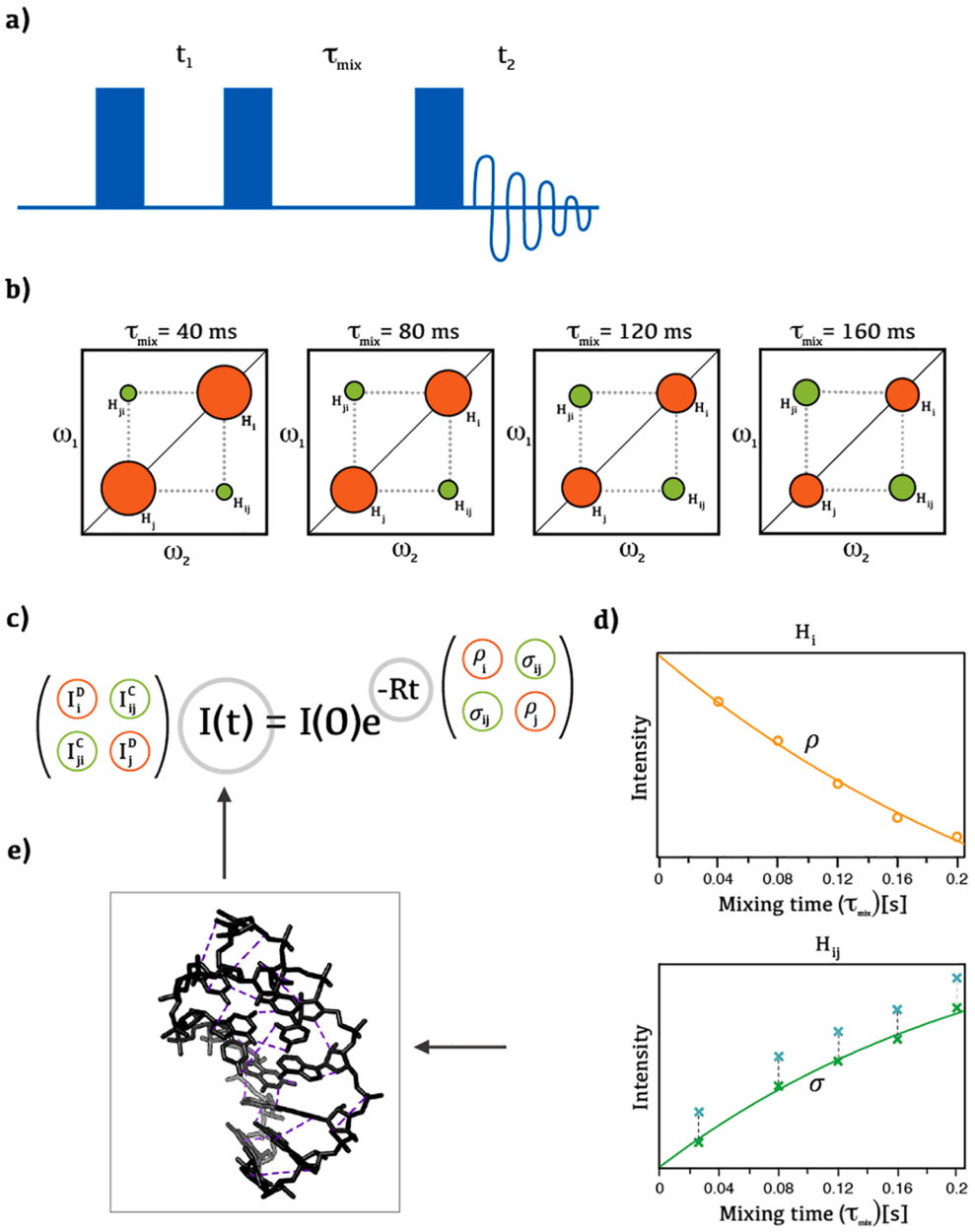

Fig. 1. Schematic of the eNOE protocol. A) The 2D NOESY pulse sequence: an initial 90° pulse is followed by t_1 evolution period, a second 90° pulse is followed by the variable τ_{mix} mixing time, and a final 90° pulse is followed by the t_2 detection period. B) A schematic of coupled spins in the NOESY buildup series. Diagonal peak intensities decay (orange) and cross-peak intensities buildup (green) with increasing mixing times. C) The Solomon equations for a two-spin system are used to analyze NOESY experiments. The relation between coupled spins is depicted with intensity (I) and relaxation (R) matrices. Diagonal peaks are circled in orange and cross peaks in green. D) The diagonal peak intensity decay with increasing mixing times is fit to a mono-exponential curve (top). The extracted auto-relaxation rate (ρ) and initial intensity I_0 at zero τ_{mix} are used to solve for the cross-relaxation rate (σ) (bottom) using the two-spin system calculation. The cross-peak buildup is corrected for spin diffusion, using a previously solved or conventional NOE structure to correct peak intensities, in an iterative process. The σ rate is then converted to an exact distance for use in structure calculation. E) Schematic of eNOE distance restraints (purple) mapped onto the high-resolution structure of the UUCG tetraloop (PDB: 6by4). (For interpretation of the references to colour in this figure legend, the reader is referred to the web version of this article.)

2. eNOE protocol and advantages over conventional NOE

The eNOE protocol enables calculation of the distance between two spins in a molecule within 0.1 Å accuracy given favorable conditions [30,31]. A time- and ensemble-averaged quantity, eNOE measurements enable the resolution of spatial sampling through multi-state structure calculations [32,33]. Highly accurate protein and RNA structure calculations based on eNOEs alone are comparable to using conventional NOEs with added restraints from *J* couplings and residual dipolar couplings (RDCs) [34–36].

The advantage of the eNOE over the conventional NOE arises from two main differences in the protocol: a measurement approach using a NOESY buildup series and spin diffusion correction. To understand the gain of the eNOE over the conventional NOE, an overview of NOE theory and drawbacks of the conventional NOE in structure calculation will first be discussed, followed by a deeper discussion of the eNOE theory and protocol. Of note to the inquisitive reader, NOE theory and advancements are well-reviewed in the literature [37–39].

2.1. NOE theory and challenges in conventional NOE structure calculation

The NOE was originally described as the enhanced polarization of a nuclear spin, driven by saturation of electron spin resonance, as directly in proportion to the ratio of the nuclear and electron gyromagnetic ratios. Theoretically proposed by Albert Overhauser in 1953 as pertinent to the nuclei of metal with saturated electrons [40], the NOE was experimentally demonstrated in metals that same year by Carver and Slichter [41]. The Solomon equations, published in 1955, expanded the NOE interaction to nuclear spin–spin couplings [42]. The 25-year span between the innovation of the Solomon equations and the 2D NOESY pulse sequence for measurement of the transient NOE in 1979 [43–45] included the first study of small molecule dynamics in 1965 [5] and small molecule-protein binding and conformations in 1972 by 1D steady-state NOE measurements [6,7].

NOE measurements in macromolecules depend on the 2D NOESY pulse sequence as the basic building block (Fig. 1A) [44,45]. Comprised of three 90° pulses, a t_1 evolution period follows the first 90° pulse,

during which magnetization in the transverse plane is labeled by its chemical shift. Then, a mixing period, usually referred to as τ_{mix}, follows the second 90° pulse, where longitudinal magnetization experiences cross relaxation. Data acquisition follows the third 90° pulse, where transverse magnetization is observed as a function of t_2 delay time [45].

The τ_{mix} mixing period allows for cross relaxation, or polarization transfer between spin-active nuclei in a molecule. The NOE cross-relaxation rate, σ, is related to the distance, r, between spins by the proportionality $\sigma \propto r^{-6}$ [41]. Analysis of NOE experimental data relies on the Solomon equations for the two-spin system (Fig. 1C), which describe the relation of diagonal- and cross-peak intensity (I^d and I^c, respectively) as a function of time t to the auto- and cross-relaxation rates (ρ and σ, respectively, and more broadly R) between coupled spins [42]:

$$I(t) = I(0)e^{-Rt} \tag{1.0}$$

where I and R are the peak intensity and relaxation matrices. Equation (1.0) can be readily understood by writing out I and R for the two-spin system to show the relation between spin 1 and spin 2:

$$\begin{bmatrix} I_1^d & I_{12}^c \\ I_{21}^c & I_2^d \end{bmatrix}(t) = \begin{bmatrix} I_1^d(0) & 0 \\ 0 & I_2^d(0) \end{bmatrix} exp\left(- \begin{bmatrix} \rho_1 & \sigma_{12} \\ \sigma_{12} & \rho_2 \end{bmatrix} t \right) \tag{1.1}$$

In practice, there are many more than two spins interacting in a molecule. Expansion of the two-spin system in matrix representation to a macromolecular spin system, with hundreds to thousands of spins, illustrates the challenge of spin diffusion, indirect magnetization transfer from neighboring spins, in NOE analysis [46–48]. Equation (1.2) depicts a third spin affecting the relation between spin 1 and spin 2 via coupling of σ_{13} and σ_{23}:

$$\begin{bmatrix} I_1^d & I_{12}^c & I_{13}^c \\ I_{21}^c & I_2^d & I_{23}^c \\ I_{31}^c & I_{32}^c & I_3^d \end{bmatrix}(t) = \begin{bmatrix} I_1^d(0) & 0 & 0 \\ 0 & I_2^d(0) & 0 \\ 0 & 0 & I_3^d(0) \end{bmatrix} exp\left(- \begin{bmatrix} \rho_1 & \sigma_{12} & \sigma_{13} \\ \sigma_{12} & \rho_2 & \sigma_{23} \\ \sigma_{13} & \sigma_{23} & \rho_3 \end{bmatrix} t \right) \tag{1.2}$$

In addition to neglecting spin diffusion, another disadvantage of conventional NOE structure calculation is the use of generously estimated upper-limit distance restraints rather than exact distances, and no lower-limit distance restraints. This protocol was introduced in the 1980 s due to low spectrometer sensitivity and resulted in loose distance restraints [37,49].

2.2. Principles of the eNOE method

The eNOE protocol begins with the NOESY buildup, measured by a series of NOESY experiments conducted at increasing τ_{mix} mixing times (Fig. 1B) [49]. The application of a buildup series to protein and nucleic acid NOESY experiments is unique to the eNOE method [1]. The maximum τ_{mix} is specifically chosen for each molecule to minimize spin diffusion, and is inversely proportional to the tumbling time, τ_c, of the molecule. That is, the greater τ_c the lower the maximum τ_{mix}. This translates to a theoretical maximum τ_{mix} mixing time of 2.5×10^{-10} s^2 τ_c^{-1} for proteins and $4 \times 10^{-10} s^2$ τ_c^{-1} for RNA [30,36].

The change in NOE peak intensities with increasing τ_{mix} mixing times provides the information needed to calculate exact distance restraints. The diagonal peak intensity as a function of increasing τ_{mix} requires fitting to an exponential decay curve, a close approximation to the exact solution, to obtain the auto-relaxation rate (ρ) and initial intensity I_0 (Fig. 1D, top) [30]:

$$\frac{I_{ii}(t)}{I_{ii}(0)} = e^{-\rho_i t} \tag{2.0}$$

The extracted ρ and I_0 values are inserted into the two-spin system description of the diagonal peak intensity in equation (2.1) at each mixing time t to fit the cross-relaxation rate (σ) (Fig. 1D, bottom) [50]:

$$\frac{I_{ij}(t)}{I_{ii}(0)} = -\frac{\sigma_{ij}}{\lambda_+ - \lambda_-}\left(e^{-\lambda_- t} - e^{-\lambda_+ t}\right) \tag{2.1}$$

where:

$$\lambda_\pm = \frac{\rho_i + \rho_j}{2} \pm \sqrt{\left(\frac{\rho_i - \rho_j}{2}\right)^2 + \sigma_{ij}^2} \tag{2.2}$$

To account for spin diffusion, the spin diffusion correction factor, p, is calculated as the ratio of the peak intensities in the full spin matrix and two-spin simulation. p is then used to scale the measured buildup intensities I^{app},using equation 3.0 [15]:

$$I_{ij}(t) = p_{ij}(t) I_{ij}^{app}(t) \tag{3}$$

The simulations are conducted with a known structure of the highest possible resolution (Fig. 1E) [51]. Initially, any kind of structure may be used, but once an initial eNOE structure is obtained it can be used for further refinement. In this way, the eNOE protocol is an iterative process, where the resultant structure is used to improve subsequent structure calculations. The corrected intensity I is applied to equation (1.0).

The resultant buildup curves are empirically inspected for adequate fit to the intensity data or alternatively, the residuals or a correlation coefficient may be used. The cross-relaxation rate (σ) is then converted to an effective distance (r_{ij}^{eff}), a single value that absorbs motional effects, using equation 4.0 [30]:

$$r_{ij}^{eff} = \left(\left(\frac{\mu_0}{4\pi}\right)^2 \frac{\gamma^4 \hbar^2}{10} \frac{\tau_c}{\sigma_{ij}}\right)^{1/6} = \left(56.94 \frac{\tau_c/ns}{\sigma_{ij}/s^{-1}}\right)^{1/6} \tag{4}$$

In practice, there are sources of error originating from different magnetization pathways during the pulse sequence. To prevent over-restraining of distances in structure calculations, the following tolerances are given: if the evaluated cross-peak buildup rates are bidirectional, meaning normalized to both diagonals and providing both σ_{ij} and σ_{ji}, the upper and lower distance limits are set to r_{ij}^{eff} for structure calculation. In that case, the two individually obtained cross-relaxation rates σ_{ij} and σ_{ji} are used to form a geometric mean. If the rates are unidirectional, meaning only one cross-peak buildup can be evaluated, commonly due to spectral overlap of a pertinent diagonal peak, the upper and lower distance limits are given tabulated limits (either +/− 20 % or using the values listed in Strotz et al. [52]). In cases where neither diagonal is usable to normalize the buildups, a generic normalized NOE can be extracted from the cross-peak buildup using averaged auto-relaxation rate (ρ) and upper limit intensity(I_0^{upper}) values, providing an upper limit distance restraint which does not violate the true distance [53].

3. Technical advancements of the eNOE

Since the last eNOE review in 2018 [54], there have been considerable technical advancements to the eNOE, including pulse sequence innovations to improve assignment and spectral quality, adapting the eNOE protocol to proton-detected solid-state NMR and addressing NOESY buildup measurement time. Integration of eNOE analysis into Bruker Dynamics Center software has expanded accessibility. Further, the eNOE has proved a reliable benchmark in assessing spatial samplings and an integral tool in novel methods to elucidate molecular motion. The following section details these recent advancements.

3.1. Novel pulse sequences

A quantitative approach, the eNOE method is particularly dependent on pulse sequences with the highest possible signal-to-noise ratio, minimal peak overlap and magnetization transfer depending exclusively on dipole–dipole cross relaxation. Several developments have improved these aspects of eNOE recording.

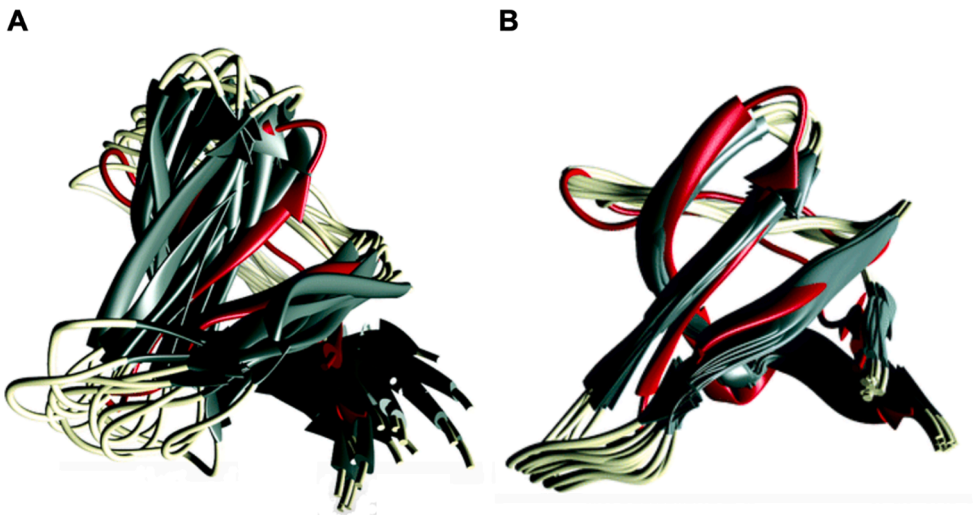

Fig. 2. The eRFDR approach improves the accuracy of structure calculation from solid-state NMR. A) Structural ensemble of the 10 lowest-energy models, calculated using conventional upper-distance restraints. B) Structure calculation of the lowest energy models calculated with 30 bidirectional, 35 unidirectional, and 47 conventional upper-distance eRFDR restraints. *With permission from Chem Commun., 55, Grohe et al., Exact distance measurements for structure and dynamics in solid proteins by fast-magic-angle-spinning NMR, Copyright Royal Society of Chemistry (2019).*

3.1.1. EASY-ROESY for congested spectral regions of medium-sized constructs

The ROESY experiment, short for Rotating frame Overhauser Effect Spectroscopy, is like the NOESY in that it probes dipole–dipole driven magnetization transfer between nearby protons. However, the cross relaxation occurs between spins that are spin locked in the transverse plane, relaying a different dependence on the spectral density functions. ROESY is preferably applied to small constructs, as it avoids the near cancellation of cross relaxation in NOESY when $\omega_o\tau_c \approx 1$ (ω_0 is the Larmor frequency). In contrast to NOESY, ROESY has unwanted *J*-coupling driven TOCSY transfer. This is particularly unfortunate when the cross-relaxation rate is quantified in an exact way ('eROE'). The EASY-ROESY improves on the quantification and TOCSY suppression of the ROESY using two bracketed, off-resonance adiabatic spin locks [55]. Ilgen and coauthors introduce further improvements to the EASY-ROESY experiment; most notably, pure shift homonuclear decoupling is introduced in the indirect dimension to reduce signal overlap, and gradient selected F1-PSYCHE-EASY-ROESY to reduce t_1 noise [47,48,56]. A drawback of these implementations is the loss of longer distance cross peaks, which may be pushed under the noise level. To address this, Ilgen and coauthors implement gradient selected *F1-perfect*BASH-EASY-ROESY, enhancing sensitivity, yielding new cross peaks at higher mixing times, and allowing for the quantification of cross relaxation [47].

3.1.2. 3D HETMAT for labile proton assignment of nucleic acids

The introduction of a new 3D heteronuclear magnetization transfer (HETMAT) pulse sequence for the assignment of labile protons is of particular benefit with larger RNA. The nucleic acid NOESY is challenged by low cross-peak signal to noise and poor observation of imino peaks resultant from solvent exchange [57,58]. A pseudo 3D HSQC NOESY, the HETMAT pulse sequence employs selective longitudinal cross polarization specific for ^{1}H-^{15}N frequency pairs in ^{15}N labeled samples, along with cross-peak enhancement through repeated τ_{mix} mixing periods and water suppression [59]. This results in signal enhancement by a factor of two to five compared to the 2D NOESY.

This method is not suited to yield the many hundreds of eNOEs required for a structure calculation. However, it may be attractive to interrogate specific interproton distances when the proton and bound ^{15}N chemical shifts are known. Cross-peak buildups could then be normalized in the same way as generic normalized NOE [53] to obtain upper distance limits.

3.1.3. Super resolution NOESY for large biomolecules

Large biomolecules present a challenge to NOE structure calculation through an increased number of spin resonances and tumbling time (τ_c), causing broadened resonances and hindering resolution. The super resolution pulse sequence increments the NOESY t_1 evolution period simultaneously with the τ_{mix} mixing period [60]:

$$\tau_{mix} = \sum_{i=0}^{N} a_i t_1^i \quad (5)$$

In a conventional NOESY experiment, τ_{mix} is independent of the t_1 evolution period, so $N = 0$ and $a_0 = \tau_{mix}$. The super resolution NOESY creates a dependency of τ_{mix} on t_1, which can be linear, where $N = 1$, or quadratic, where $N = 2$. At shorter τ_{mix}, spin diffusion is minimized, while lengthening τ_{mix} allows for NOE buildups and the accurate determination of NOE distances. This approach results in average cross-peak linewidth reductions of 16–32 % and corresponding enhanced resolution, enabling the resolution of cross peaks that were not observed in a conventional NOESY experiment.

While cross-peaks linewidths are generally reduced, diagonal peaks are typically broader. How these modifications to peak intensity impact exact distance extraction remains to be investigated.

3.2. Exact distance restraints from solid-state NMR

Grohe and coauthors adapt the eNOE framework to proton-detected solid-state NMR to improve the accuracy of distance restraints used in determination of protein structure [61]. The authors use a deuterated, ^{15}N- and ^{13}C-labeled α-spectrin SH3 domain to measure homonuclear dipole–dipole magnetization transfer with a 3D ^{15}N-edited radio frequency-driven recoupling (RFDR) pulse scheme (H-RFDR-hNH). As with solution-state NOEs, the accuracy of extracted solid-state proton-proton distances is impeded by several factors, including site-specific magnetization loss during mixing and spin diffusion. Using an eRFDR processing protocol like that of the solution-state eNOE, Grohe and co-authors compensate for reduced differential transfer efficiency during correlation by normalizing cross-peak intensity to the diagonal peak intensity at I_0 (see Equation (1.0)). They account for magnetization loss by correcting cross-peak buildups using a fixed, diagonal decay rate, and offset spin diffusion using correction factors based on transfer matrix simulations. eRFDR distance restraints result in more accurate structure calculation than conventional RFDR calculation, and reduce the backbone structure RMSD from 2.40 Å to 0.56 Å as applied to the SH3 domain (Fig. 2A and 2B) [61].

3.3. Non-uniform sampling

As explained in Section 2, the eNOE protocol relies on the

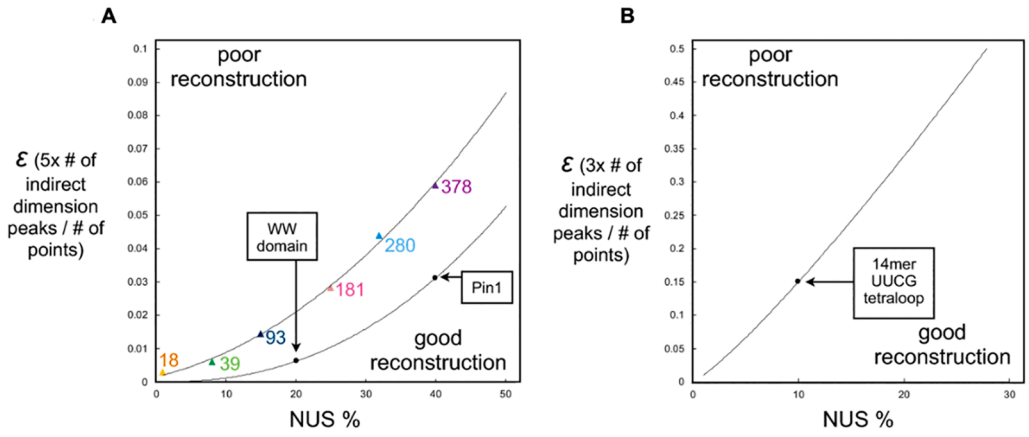

Fig. 3. Effect of NUS sparsity on eNOE yield and guidelines for successful eNOE analysis. A) Sparsity fraction (ε) versus NUS percent sampled for 3D NOESY measurement. The cases of the full-length Pin1 construct and WW domain are indicated. Values right of the curve indicate good reconstruction. B) Sparsity fraction (ε) versus NUS percent sampled for 2D NOESY measurement; the 14-mer UUCG tetraloop RNA is indicated. *With permission from J. Biomol. NMR, 74, Nichols et al., Reducing the measurement time of exact NOEs by non-uniform sampling, Copyright Springer Nature (2020).*

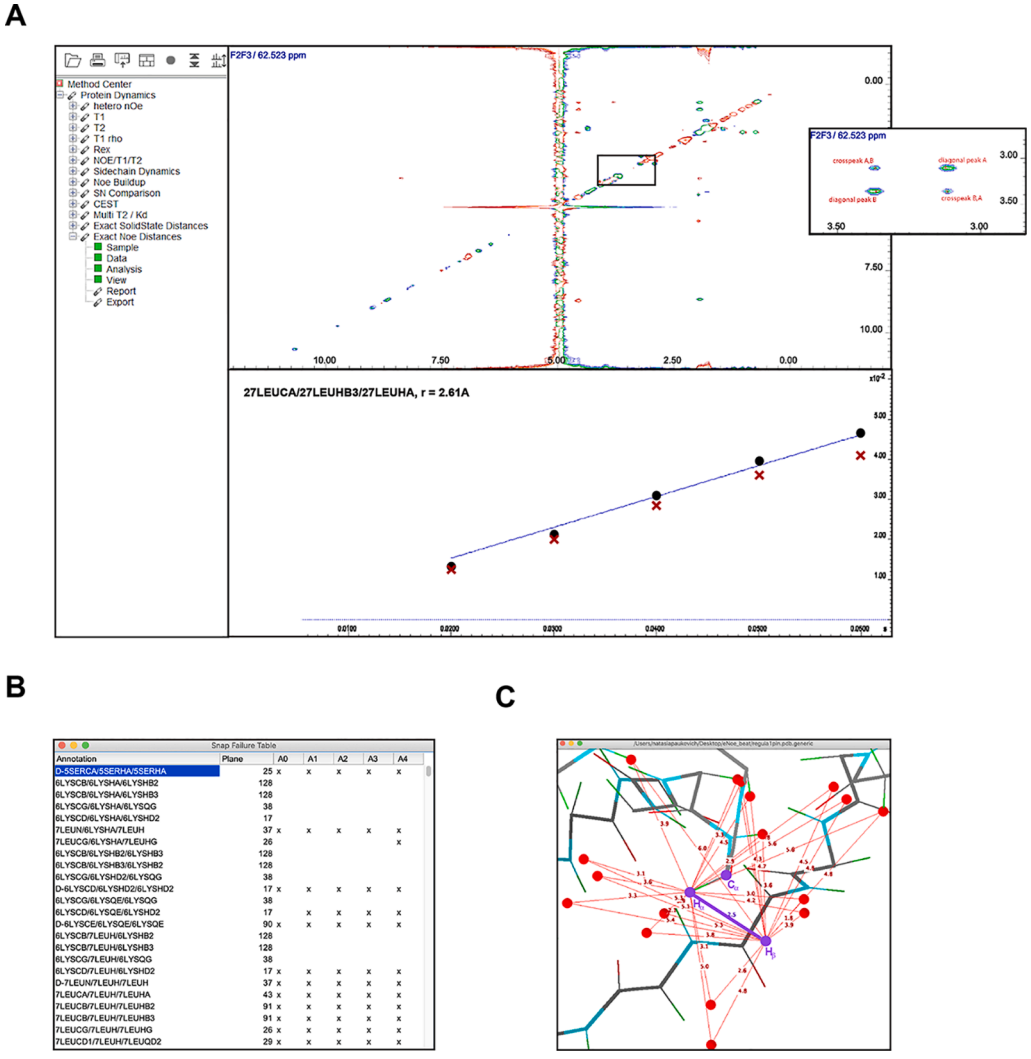

Fig. 4. The eNOE analysis integrated in the Bruker Dynamics Center interface. A) Screenshot of the Dynamics Center main window. A spectrum, zoomed into a region of cross peaks and diagonals. B) eNOE buildup curve with mixing times on the x-axis. Raw values (black circles) and spin diffusion adjusted values (red crosses). C) The Snap Failure Table displays a list of buildup curves, detailing the peaks missing at each mixing time. D) Structure model panel showing Cα, Hα, and $H\beta_3$ atoms highlighted in purple. The eNOE of interest is highlighted in purple. Atoms within a 6 Å radius potentially contributing to spin diffusion are depicted in red. (For interpretation of the references to colour in this figure legend, the reader is referred to the web version of this article.)

measurement of a buildup series of NOESY spectra. While a 2D [^{1}H–^{1}H] buildup series may require just a few days, a 3D [^{13}C;^{15}N]-resolved buildup series may take upwards of 10 days, a prohibitive time constraint. Nichols and coauthors implement a Poisson gap non-uniform sampling (NUS) scheme to reduce measurement time by sampling a subset of points in the indirect dimensions, applicable to spectra at all mixing times in context of the NOESY buildup once an assignment is completed from a linearly sampled spectrum [62].

The authors determine optimal NUS sampling percentages for a reliable reconstruction using eNOE yield and the quality of extracted distances. The authors test 3D NOESY spectra using the full-length, 163-residue Pin1 protein and the 34-residue WW domain of Pin1, and 2D NOESY using the 14-nucleotide UUCG tetraloop RNA. The quality of extracted distances is conserved to 10 % sampling in all cases. However,

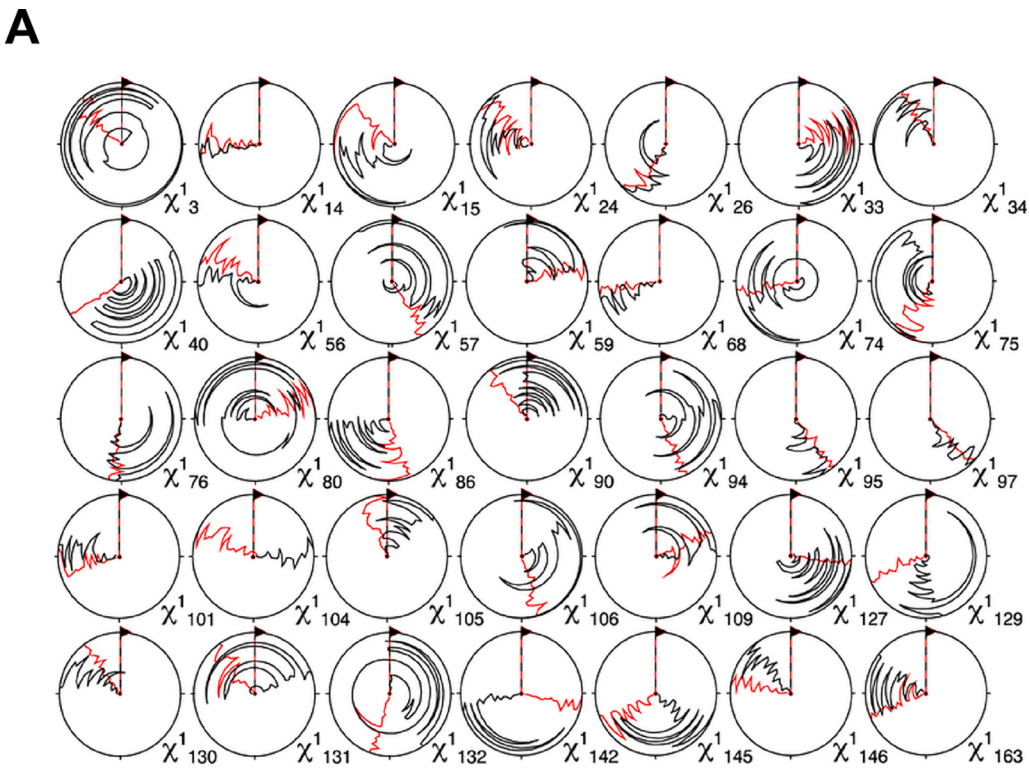

Fig. 5. Stereospecific resonance assignment from combined eNOEs and *J* couplings. The residue-specific circle plots depict χ^1 angles. The angle distributions are highly varied in structures calculated using eNOEs and $J_{H\alpha\text{-}H\beta}$ couplings (black) and are significantly narrowed upon stereospecific assignment of methylene protons (red). *Published in Magnetochemistry, 4, Born et al., Efficient stereospecific Hβ2/3 NMR assignment strategy for mid-size proteins, Copyright MDPI (2018).* (For interpretation of the references to colour in this figure legend, the reader is referred to the web version of this article.)

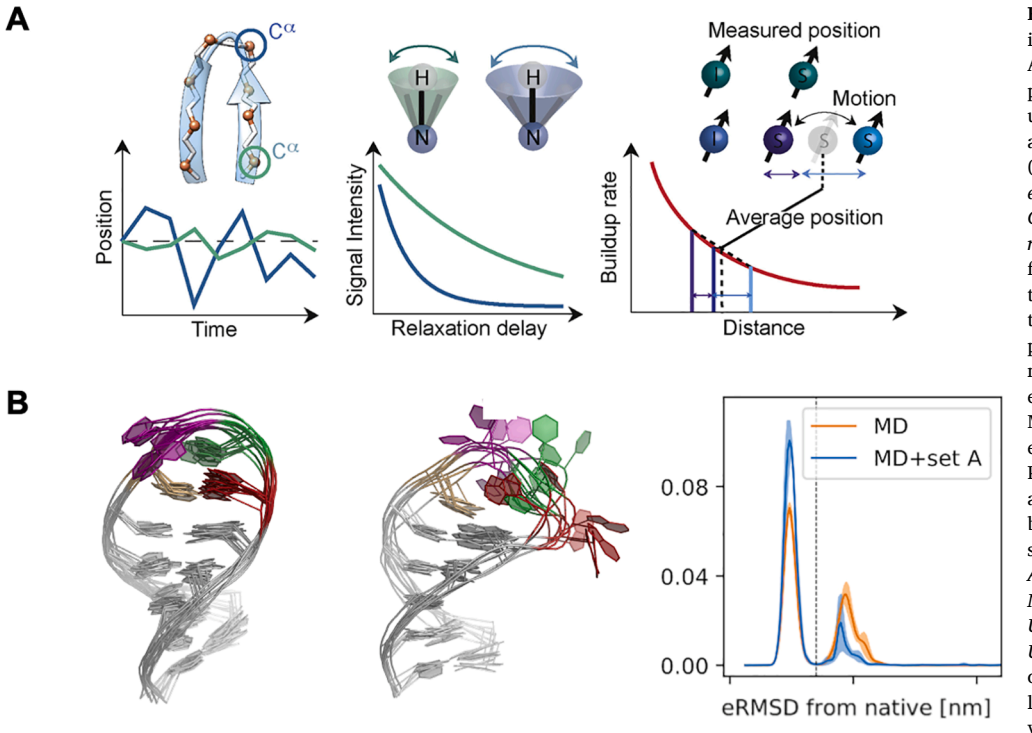

Fig. 6. eNOEs as a benchmark for assessing spatial samplings in protein and RNA. A) Graphic depicting complementary experiments sensitive to dynamics; MD simulations (left), NMR relaxation (middle), and multi-state eNOE structure calculation (right). *Published in Structure, 28, Grohe et al., Protein Motional Details Revealed by Complementary Structural Biology Techniques, Copyright Elsevier (2020).*B) Conformations of consensus state A (left) and the base flip, alternate state B of the UUCG tetraloop RNA (center); histogram of the populations of states A and B, based on the nucleic acid-specific distance metric eRMSD from native (right). The original MD simulation (orange) compared to the eNOE-refined ensemble (MD + set A, blue). Population distribution is on the vertical axis. Vertical dashed line shows separation between states A and B. Shadows show standard error. *With permission from Nucleic Acids Res., 48, Bottaro et al., Integrating NMR and simulations reveals motions in the UUCG tetraloopniques, Copyright Oxford University Press (2020).* (For interpretation of the references to colour in this figure legend, the reader is referred to the web version of this article.)

decreased eNOE yield results in compromised structures and practically sets the NUS reconstruction cutoff to 40 % for the full Pin1, 20 % for the WW domain, and 10 % for the UUCG tetraloop. These findings are theoretically rationalized and generalized by applying the sparsity fraction ε as the measure of reconstruction success (Fig. 3Aand 3B):

$$\varepsilon = \frac{k}{N} \tag{6}$$

where k is the degrees of freedom determined by the number of indirection dimensions in the spectrum (5x or 3x the number of peaks in the indirect dimensions for 3D and 2D, respectively) and N the number of points measured in the linear sampling case. Given a typical scenario, 50 % NUS provides a safe cutoff.

Wieske and Erdélyi [63] evaluate the effect of Poisson gap and random-shuffle NUS schemes on both 2D NOESY buildups and

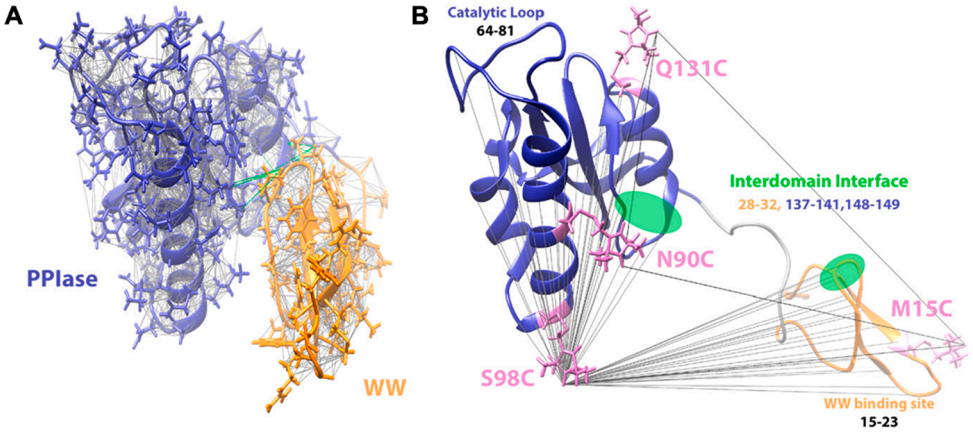

Fig. 7. Different NMR probes used to reveal inter- and intradomain dynamics highlighted in compact and extended states of Pin1. A) eNOE distances and interdomain NOEs are mapped in gray and green, respectively, on the crystal structure of the compact state of Pin1 (PDB: 1pin). PPIase domain in blue and WW domain in orange. B) DEER and PRE (arising from mutant S98C) restraints are mapped in black and gray, respectively, on an NMR structure of Pin1 in the extended state (PDB: 1nmv). *Reprinted with permission from J. Am. Chem. Soc., 143, Born et al., Reconstruction of Coupled Intra- And Interdomain Protein Motion from Nuclear and Electron Magnetic Resonance. Copyright 2021 American Chemical Society.* (For interpretation of the references to colour in this figure legend, the reader is referred to the web version of this article.)

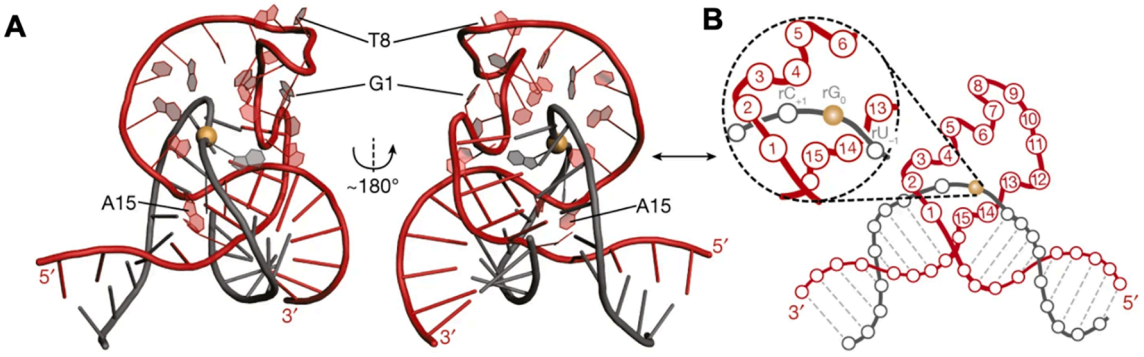

Fig. 8. The DNAzyme compact core locks in substrate RNA. A) Ab-initio NMR structure of the precatalytic Dz^{5C}–$RNA^{2'F}$ complex. The DNA is shown in red and the RNA in grey, respectively. B) The precatalytic complex depicts a winding of the catalytic loop around substrate RNA. *With permission from Nature, 601, Borggräfe et al., Time-resolved structural analysis of an RNA-cleaving DNA catalyst, Copyright Springer Nature (2022).* (For interpretation of the references to colour in this figure legend, the reader is referred to the web version of this article.)

standalone 2D NOESY spectra of small molecules. They acquired spectra in 25 % NUS sampling increments, resulting in progressively reduced accuracy of experimentally derived internuclear distances (using the linear buildup approximation) with decreased sampling. The authors report a Lin's concordance coefficient (r_c) assessment of buildup curve reproducibility dropping from 0.95 for uniformly sampled buildup data at all experimental distances to 0.75 for 75 %, 0.68 for 50 %, and 0.35 for 25 % random-shuffle sampling with modified iterative thresholding (MIST) reconstruction. In agreement with Nichols and coauthors [62], weak NOE intensities are more severely affected than strong NOEs [63].

3.4. Integration of eNOE analysis in Bruker dynamics Center software

An eNOE protocol is now integrated into the Bruker Dynamics Center software[1] (Fig. 4A). The user can assign a NOESY spectrum (the spectrum with the longest τ_{mix} is recommended) within the Bruker software or import an assignment from a preferred software. The buildup series is then analyzed to obtain cross-relaxation σ rates, which are corrected for spin diffusion using a prior PDB structure (Fig. 4B). The obtained σ rates are converted to distances, complete with fitting parameters, for export in the users' preferred structure calculation program. Notably, the software is interactive, allowing the user to visualize and highlight proton-proton couplings in graphical data representations and the PDB simultaneously (Fig. 4C and 4D).

[1] Version 2.8.1 is available at: https://www.bruker.com/de/products-and-solutions/mr/nmr-software/dynamics-center.html.

3.5. Improved stereospecific assignments with eNOEs

Methylene proton assignment is often obtained with a combination of three-bond H^{α}–H^{β} *J* couplings and NOEs [37]. It was previously demonstrated that eNOEs are superior to conventional NOEs in stereospecific methylene assignment of a small, 56 residue protein [64]. Born and coauthors [65] improve the stereospecific assignment of methylene $H^{\beta 2}$ and $H^{\beta 3}$ protons through a modification of the 3D HACAHB-COSY pulse sequence [66], combined with eNOEs.

Using the Pin1 construct in a structure calculation, the authors report the contribution of conventional NOEs, eNOEs and $^3J_{H\alpha-H\beta}$ couplings in stereospecific assignment of methylene protons. While conventional NOEs and $^3J_{H\alpha-H\beta}$ couplings combined yield 66 stereospecific methylene proton assignments, conventional NOEs alone provide no assignments. Replacing conventional NOEs with eNOEs in combination with $^3J_{H\alpha-H\beta}$ couplings yields 114 assignments. eNOEs alone define stereochemistry at most assigned methylene protons, a significant improvement amounting to 45 % assignment of methylene protons. Further, χ_1 dihedral angle distributions (Fig. 5) are narrowed in structure calculations using stereospecific assignment in combination with eNOEs and $^3J_{H\alpha-H\beta}$ couplings versus without stereospecific assignment.

3.6. eNOEs as a benchmark in spatial samplings

3.6.1. Spatial sampling of proteins

The eNOE protocol outputs static structural ensembles describing motion through all-atom distributions. Grohe and coauthors compare protein motion information from eNOE ensembles to unbiased

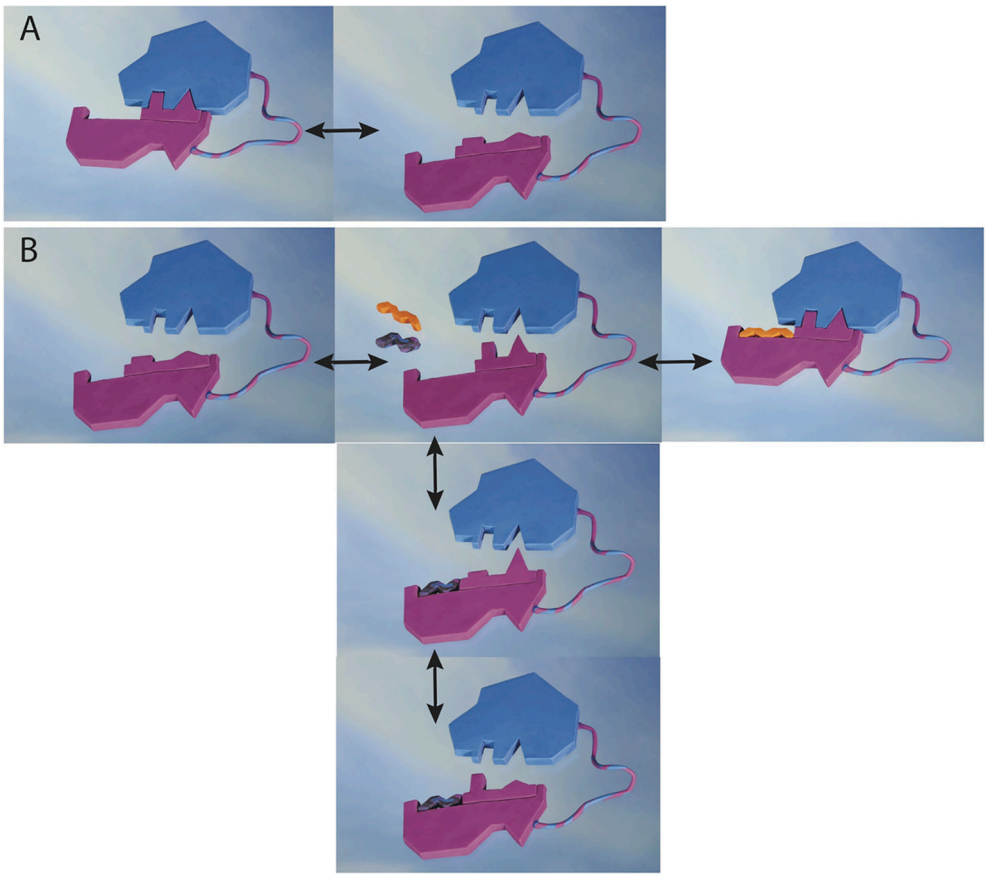

Fig. 9. WW domain allostery in the apo state and in the presence of activator and repressor ligands. A) The apo WW domain (pink) undergoes micro-millisecond exchange between two conformations, one of which permits interaction with the catalytic PPIase domain (blue). B) The presence of repressor (orange) or activator (gray) ligand alters the allosteric propensity towards enhanced interaction with the PPIase or a clash between the domains, respectively. *Published in Angew Chem Int Ed, Volume: 59, Strotz et al., Protein Allostery at Atomic Resolution, Copyright Wiley (2020)*. (For interpretation of the references to colour in this figure legend, the reader is referred to the web version of this article.)

molecular dynamics (MD) simulations, solution- and solid-state NMR relaxation data, and MD simulations incorporating eNOE bias potentials (Fig. 6A) [46]. Importantly, these techniques are orthogonal and detect motion on different timescales, with varied range of distance and applied to all atoms or only the backbone. Yet, the distinct techniques independently confirm the identified protein structural dynamics and further, prove complimentary to one another by alleviating shortcomings. For example, concerns about the accuracy of MD simulations are mitigated in combination with experimental NMR restraints [67,68], while MD simulations afford a global energy expression of protein dynamics in combination with the eNOE, which imparts local distance information [46].

Beyond complementarity, eNOEs serve as a reliable benchmark in spatial samplings. Similar to Grohe and coauthors' independent confirmation of measured cross-relaxation rates [46], Kuprov and coauthors apply NOE proton-proton cross-relaxation rates as a benchmark to assess the accuracy of MD trajectories in the creation of the Spinach software to convert MD trajectory data to a relaxation superoperator [69]. Vasile and Tiana develop a method to account for spin diffusion in flexible molecule conformation ensembles, relying on NOE intensities obtained from a complete relaxation solution as input in MD simulations to sample molecular conformations at maximum entropy [70].

3.6.2. *Spatial sampling of nucleic acids*

NMR of nucleic acids has its own set of challenges compared to proteins. The proton density is lower, limiting the efficacy of interproton restraints [71,72], and RDC and *J* coupling measurements are more challenging to obtain [54]. Further, spin labeling is expensive, and MD force fields are less established for nucleic acids than for proteins. As a result, nucleic acid structure calculations may rely on several methods to approximate conformation [73].

The 2018 eNOE structure of the UUCG tetraloop RNA construct [36], discussed thoroughly in a prior review [29], demonstrates a high-resolution structure may be achieved with NOESY experiments alone, as compared to the effort enacted in prior calculations of the same, well-characterized structure using a combined conventional NOEs, RDCs and *J* coupling measurement approach [74,75]. While the 2018 effort yielded a multi-state eNOE structure of RNA, the UUCG tetraloop is a relatively static model construct. To demonstrate internal motions absent extensive relaxation data, MD simulations may be used.

In a comparison of UUCG tetraloop eNOE versus conventional NOE distance restraints as supplements in AMBER structure refinements, eNOEs result in more accurate RDC-based statistics [54]. Alternate states can further be characterized with MD simulations alongside eNOE experimental restraints. MD simulations of nucleic acids are comparatively less established than protein MD simulations, and Bottaro and coauthors report eNOEs can serve as a benchmark to validate MD simulations [76]. The eNOE UUCG tetraloop data was used alongside MD simulations to reveal a low populated, base flip alternate state (Fig. 6B). In this approach, eNOEs were used to reweight *a posteriori* the ensemble generated via enhanced sampling MD simulations (Fig. 6C). The population of this minor, alternate state is almost completely retained after reweighting with eNOEs, and therefore consistent with experimental distance restraints [76].

3.7. *eNOEs and structural ensembles*

Macromolecular motion, omnipresent in biological processes, can be challenging to study as many NMR dynamics methods probe exclusively local motional data, while structural methods traditionally elucidate fixed states. Recent NMR advancements contribute to the study of protein allostery and other macromolecular motions, including the integration of eNOEs with other magnetic resonance methods and MD simulations (discussed in Section 3.6).

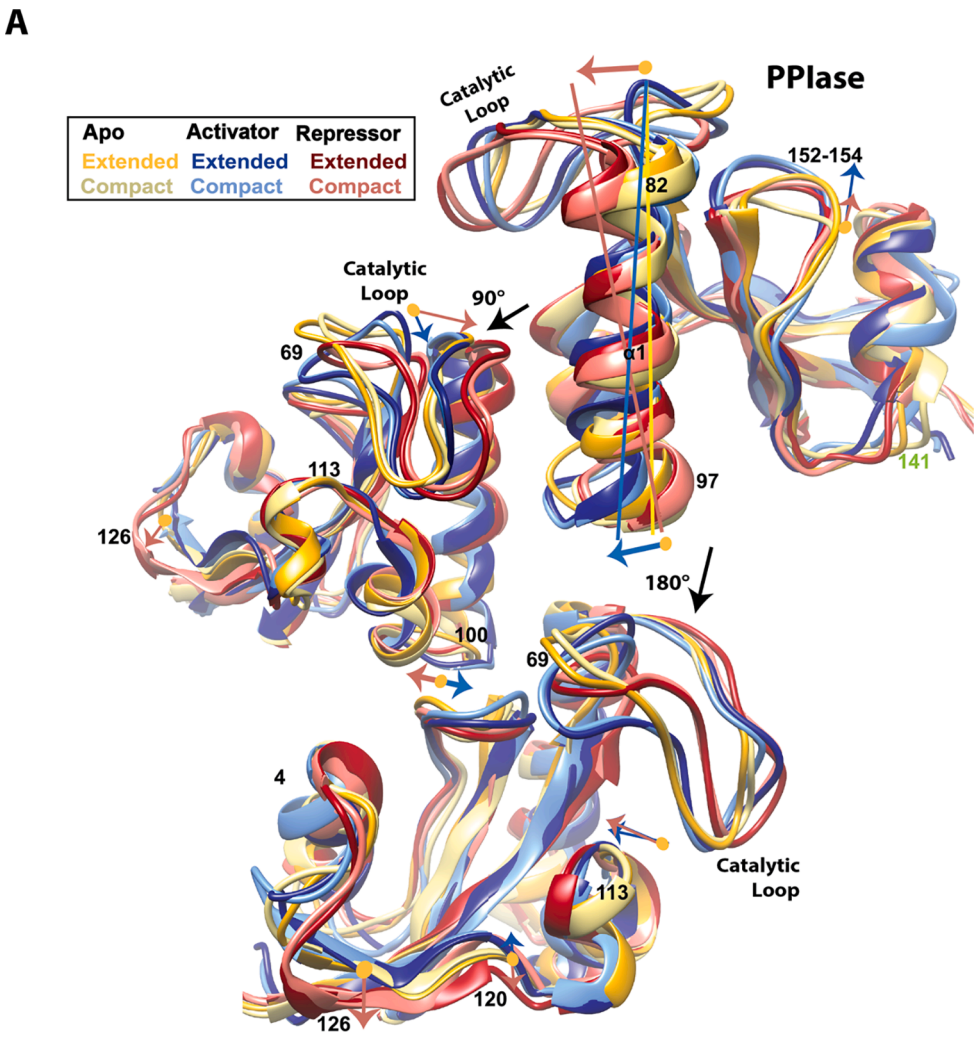

Fig. 10. eNOEs contribute to discernment between structures of apo, repressor- and activator-bound PPIase domain. A) Mean two-state structures of the PPIase apo (yellows), bound to activator ligand (blues), and repressor ligand (reds). Structure on left is domain rotated 90°, and structure on the bottom is rotated 180°. Note red and blue arrows at points where activator and repressor-bound structures deviate from apo (yellow circles). *Reprinted with permission from Born et al., 2022.* (For interpretation of the references to colour in this figure legend, the reader is referred to the web version of this article.)

Born and coauthors [77], establish a novel method probing the coupling of intra- and interdomain dynamics, and describe how changes to intradomain structures alter interdomain sampling, and vice versa. This new method of protein motional modeling combines time-averaged NMR and distance distribution-resolving EPR restraints: eNOEs, *J* couplings and RDCs in intradomain calculations, and paramagnetic relaxation enhancement (PRE), RDCs and double electron–electron resonance (DEER) to model interdomain distributions (Fig. 7A and 7B). While *J* couplings and RDCs provide angles, eNOEs yield precise short-range distances and DEER and PRE, long-range distances. Of note, the authors detect 20 eNOE distance restraints between the two Pin1 domains; the original NMR structure failed to identify interdomain contacts [78]. Born and coauthors calculate multi-state structures, characterizing extended and compact states of domain arrangement correlated with structural ensembles of the individual domains. The biological applications of this work are discussed in Section 4.2.

A drawback of NOE structure calculation, including the eNOE, is the omission of timescales in r^{-6} NOE averaging in refinement (see Equation 4.0) [79]. This omission can be significant because, depending on the timescales of internal motions, the true averaging can deviate from r^{-6} and therefore impact the apparent distances [80–82]. Smith and coauthors address this using their Kinetic Ensemble approach, contextualizing the NOE buildup series within a structural model accounting for the hierarchy of timescales and yielding accurate τ_c tumbling times [83].

4. The eNOE in biological systems

The eNOE protocol is a powerful tool to elucidate the interplay between structure and dynamics in proteins and nucleic acids. Following an initial focus on technique development, the eNOE protocol is increasingly applied to address biological questions. In this section, the two most advanced examples are discussed.

4.1. Dnazyme complexed with RNA

Borggräfe and coauthors apply the eNOE protocol to DNA to obtain the structure of a catalytic DNAzyme, the RNA-cleaving '10-23′ type DNA sequence with notable therapeutic potential [84]. The authors use eNOEs alongside PREs and conventional NOEs as experimental restraints in calculating the 10–23 DNAzyme structure in complex with substrate RNA. To capture the DNAzyme-RNA precatalytic complex, the substrate RNA was modified to introduce a stabilizing 2′ fluorine at the rG_0 guanine of the cleavage site (Fig. 8B). The experimental restraints are employed in a loose simulated annealing structure calculation, addressing proton sparsity with a combination of homology restraints and ^{19}F saturation transfer. RDCs were then used to assess the probability of each spatial sampling cluster prior to structural refinement. Borggräfe and coauthors use this structural information to define, in addition to the high-resolution structure, the details of the DNAzyme catalytic function, where a compact core locks the substrate RNA into place and exposes the catalytic loop (Fig. 8A).

4.2. Pin1 allostery

The mitotic regulator Pin1 is highly relevant in the biology of neurodegenerative diseases and cancer [85,86]. Comprised of two globular domains, a flexible linker connects the Pin1 WW and peptidyl-prolyl isomerase (PPIase) domains. Pin1 regulates other proteins through the isomerization of prolines preceded by a phosphorylated serine or threonine, altering the regulation of post-translational modifications and protein recycling and degradation [87]. The WW domain negatively regulates catalytic activity through contacts with the PPIase domain [88]. To elucidate allosteric regulation of Pin1 at the structural level, Strotz and coauthors [89] use eNOEs and *J* couplings to calculate a high-resolution, two-state structure of the Pin1 WW domain, with one state primed to interact with the PPIase domain. The authors go on to articulate a predictive model of ligand-mediated dynamic allostery, describing a coupling of the ligand binding site on the WW domain to the WW-PPIase interface using two ligands (Fig. 9B). Binding of the 'repressor' ligand strengthens the WW-PPIase interaction by shifting the two-state distribution towards a compact domain arrangement. Alternate states of the WW domain induced by 'activator' ligand-binding clash with the PPIase domain interface, weakening the WW-PPIase interaction and favoring an extended domain arrangement [90].

Implementing their novel method described in section 3.7 [77], Born and coauthors detail ligand-based conformational changes in Pin1 interdomain allostery using the full-length construct [91]. In their initial work, Born and coauthors determine the apo Pin1 samples a 70:30 ratio of compact and extended states in the absence of ligands using EPR (Fig. 7A and 7B) [77]. The authors subsequently employ eNOEs, *J* couplings, RDCs, PRE and DEER in two-state structure calculations to determine the activator ligand employed by Strotz and coauthors [89] stabilizes an extended conformation between the two domains with no interdomain contacts [91]. In addition, hydrophobic residues of the domain interface control the sampling of structural states. Activator ligand binding to the WW domain triggers conformational changes propagating via the interdomain interface to the PPIase catalytic site, while repressor ligand binding displaces a helix in the PPIase, leading to a repositioned PPIase catalytic loop and inhibiting PPIase function (Fig. 10A).

5. Conclusion

In this review, we highlight eNOE method advancements since the last review in 2018 [11], presenting a broad scope of innovations, including spectroscopic advances, new analysis tools and synergies with other experimental methods. The eNOE method has attained a maturity that opens the door to applications with a biological focus. We believe the findings presented here are just the beginning of a wide range of systems studied using the eNOE method.

CRediT authorship contribution statement

Alya Hussain: Conceptualization, Visualization. **Natasia Paukovich:** Conceptualization, Visualization. **Morkos A. Henen:** Writing – review & editing. **Beat Vögeli:** Conceptualization, Supervision, Funding acquisition.

Declaration of Competing Interest

The authors declare that they have no known competing financial interests or personal relationships that could have appeared to influence the work reported in this paper.

Acknowledgement

We thank Conner Langeberg for critical reading of the manuscript and Dr. Alexandra Born for preparing figure templates. This work is funded by NSF grant 1917254 for Infrastructure Innovation for Biological Research, NIH Grant R01GM130694 and a start-up package from the University of Colorado to B.V.

References

[1] K. Wüthrich, NMR studies of structure and function of biological macromolecules (Nobel Lecture), in: NMR with Biol. Macromol. Solut. A Sel. Pap. Publ. from 1996 to 2020 by Kurt Wüthrich, 2021. https://doi.org/10.1142/9789811235795_0003.
[2] R. Kaiser, Use of the nuclear overhauser effect in the analysis of high-resolution nuclear magnetic resonance spectra, J. Chem. Phys. 39 (10) (1963) 2435–2442.
[3] R.A. Bell, J.K. Saunders, Correlation of the intramolecular nuclear Overhauser effect with internuclear distance, Can. J. Chem. 48 (7) (1970) 1114–1122.
[4] R.E. Schirmer, J.H. Noggle, J.P. Davis, P.A. Hart, Determination of Molecular Geometry by Quantitative Application of the Nuclear Overhauser Effect, J. Am. Chem. Soc. 92 (11) (1970) 3266–3273.
[5] F.A.L. Anet, A.J.R. Bourn, Nuclear Magnetic Resonance Spectral Assignments from Nuclear Overhauser Effects, J. Am. Chem. Soc. 87 (1965), https://doi.org/10.1021/ja00950a048.
[6] A.A. Bothner, R. Gassend, Binding of small molecules to proteins, Ann. N. Y. Acad. Sci. 222 (1) (1973) 668–676.
[7] J.P. Albrand, B. Birdsall, J. Feeney, G.C.K. Roberts, A.S.V. Burgen, The use of transferred nuclear Overhauser effects in the study of the conformations of small molecules bound to proteins, Int. J. Biol. Macromol. 1 (1) (1979) 37–41.
[8] M.D. Miller, G.N. Phillips, Moving beyond static snapshots: Protein dynamics and the Protein Data Bank, J. Biol. Chem. 296 (2021) 100749.
[9] B. Liu, H. Shi, H.M. Al-Hashimi, Developments in solution-state NMR yield broader and deeper views of the dynamic ensembles of nucleic acids, Curr. Opin. Struct. Biol. 70 (2021) 16–25.
[10] T.R. Alderson, L.E. Kay, NMR spectroscopy captures the essential role of dynamics in regulating biomolecular function, Cell 184 (3) (2021) 577–595.
[11] P. Nichols, A. Born, M. Henen, D. Strotz, J. Orts, S. Olsson, P. Güntert, C. Chi, B. Vögeli, The Exact Nuclear Overhauser Enhancement: Recent Advances, Molecules 22 (7) (2017) 1176.
[12] J.C. Kendrew, R.E. Dickerson, B.E. Strandberg, R.G. Hart, D.R. Davies, D. C. Phillips, V.C. Shore, Structure of myoglobin: A three-dimensional fourier synthesis at 2. resolution, Nature 185 (1960), https://doi.org/10.1038/185422a0.
[13] E.E. Scott, Q.H. Gibson, J.S. Olson, Mapping the Pathways for O2 Entry Into and Exit from Myoglobin, J. Biol. Chem. 276 (7) (2001) 5177–5188.
[14] A.G. Palmer, C.D. Kroenke, J.P. Loria, Nuclear magnetic resonance methods for quantifying microsecond-to-millisecond motions in biological macromolecules, Methods Enzymol. (2001), https://doi.org/10.1016/S0076-6879(01)39315-1.
[15] A. Sekhar, L.E. Kay, NMR paves the way for atomic level descriptions of sparsely populated, transiently formed biomolecular conformers, Proc. Natl. Acad. Sci. U.S. A. 110 (32) (2013) 12867–12874.
[16] K. Wüthrich, Nuclear magnetic resonance in protein research, Experientia 30 (6) (1974) 577–585.
[17] A. Masson, K. Wüthrich, Proton magnetic resonance investigation of the conformational properties of the basic pancreatic trypsin inhibitor, FEBS Lett. 31 (1) (1973) 114–118.
[18] A. Allerhand, D. Doddrell, V. Glushko, D.W. Cochran, E. Wenkert, P.J. Lawson, F.R. N. Gurd, Conformation and Segmental Motion of Native and Denatured Ribonuclease a in Solution. Application of Natural-Abundance Carbon-13 Partially Relaxed Fourier Transform Nuclear Magnetic Resonance, J. Am. Chem. Soc. 93 (2) (1971) 544–546.
[19] I.D. Campbell, C.M. Dobson, R.J.P. Williams, Proton magnetic resonance studies of the tyrosine residues of hen lysozyme assignment and detection of conformational mobility, Proc. R. Soc. London – Biol. Sci. 189 (1975), https://doi.org/10.1098/rspb.1975.0070.
[20] G.H. Snyder, R. Rowan, S. Karplus, B.D. Sykes, Complete Tyrosine Assignments in the High Field 1H Nuclear Magnetic Resonance Spectrum of the Bovine Pancreatic Trypsin Inhibitor, Biochemistry 14 (1975), https://doi.org/10.1021/bi00688a008.
[21] K. Wüthrich, G. Wagner, NMR investigations of the dynamics of the aromatic amino acid residues in the basic pancreatic trypsin inhibitor, FEBS Lett. 50 (2) (1975) 265–268.
[22] A.E. Torda, R.M. Scheek, W.F. van Gunsteren, Time-dependent distance restraints in molecular dynamics simulations, Chem. Phys. Lett. 157 (4) (1989) 289–294.
[23] A.S. Arseniev, V.I. Kondakov, V.N. Maiorov, V.F. Bystrov, NMR solution spatial structure of "short" scorpion insectotoxin I5A, FEBS Lett. 165 (1) (1984) 57–62.
[24] M.P. Williamson, T.F. Havel, K. Wüthrich, Solution conformation of proteinase inhibitor IIA from bull seminal plasma by 1H nuclear magnetic resonance and distance geometry, J. Mol. Biol. 182 (2) (1985) 295–315.
[25] W. Braun, C. Bösch, L.R. Brown, N. Gō, K. Wüthrich, Combined use of proton-proton overhauser enhancements and a distance geometry algorithm for determination of polypeptide conformations. Application to micelle-bound glucagon, BBA – Protein Struct. 667 (2) (1981) 377–396.
[26] S.W. Fesik, E.R.P. Zuiderweg, Heteronuclear three-dimensional nmr spectroscopy. A strategy for the simplification of homonuclear two-dimensional NMR spectra, J. Magn. Reson. 78 (3) (1988) 588–593.
[27] L.E. Kay, G.M. Clore, A. Bax, A.M. Gronenborn, Four-dimensional heteronuclear triple-resonance NMR spectroscopy of interleukin-1 beta in solution, Science 249 (1990) 411–414, https://doi.org/10.1126/science.2377896.
[28] K.L. Constantine, L. Mueller, M.S. Friedrichs, R.E. Bruccoleri, N.H. Andersen, H. Tong, C.F. Wandler, Structural and Dynamic Properties of a β-Hairpin-Forming

Linear Peptide. 1. Modeling Using Ensemble-Averaged Constraints, J. Am. Chem. Soc. 117 (1995), https://doi.org/10.1021/ja00149a007.
[29] P.J. Nichols, A. Born, M.A. Henen, D. Strotz, C.N. Celestine, P. Güntert, B. Vögeli, Extending the Applicability of Exact Nuclear Overhauser Enhancements to Large Proteins and RNA, ChemBioChem 19 (16) (2018) 1695–1701.
[30] B. Vögeli, The nuclear Overhauser effect from a quantitative perspective, Prog. Nucl. Magn. Reson. Spectrosc. 78 (2014) 1–46.
[31] D. Leitz, B. Vögeli, J. Greenwald, R. Riek, Temperature dependence of 1HN-1H N distances in ubiquitin as studied by exact measurements of NOEs, J. Phys. Chem. B 115 (23) (2011) 7648–7660.
[32] B. Vögeli, S. Kazemi, P. Güntert, R. Riek, Spatial elucidation of motion in proteins by ensemble-based structure calculation using exact NOEs, Nat. Struct. Mol. Biol. 19 (10) (2012) 1053–1057.
[33] B. Vögeli, P. Güntert, R. Riek, Multiple-state ensemble structure determination from eNOE spectroscopy, Mol. Phys. 111 (3) (2013) 437–454.
[34] B. Vögeli, S. Olsson, R. Riek, P. Güntert, Complementarity and congruence between exact NOEs and traditional NMR probes for spatial decoding of protein dynamics, J. Struct. Biol. 191 (3) (2015) 306–317.
[35] B. Vögeli, S. Olsson, P. Güntert, R. Riek, The Exact NOE as an Alternative in Ensemble Structure Determination, Biophys. J. 110 (1) (2016) 113–126.
[36] P.J. Nichols, M.A. Henen, A. Born, D. Strotz, P. Güntert, B. Vögeli, High-resolution small RNA structures from exact nuclear Overhauser enhancement measurements without additional restraints, Commun. Biol. 1 (2018), https://doi.org/10.1038/s42003-018-0067-x.
[37] K. Wüthrich, NMR with Proteins and Nucleic Acids, Europhys. News. 17 (1) (1986) 11–13.
[38] D.B. Davies, The nuclear overhauser effect in structural and conformational analysis, Spectrochim. Acta Part A Mol. Spectrosc. 47 (11) (1991) 1641.
[39] S. Boros, Z. Gáspári, G. Batta, Accurate NMR Determinations of Proton-Proton Distances, Annu. Reports NMR Spectrosc. (2018), https://doi.org/10.1016/bs.arnmr.2017.12.002.
[40] A.W. Overhauser, Polarization of nuclei in metals, Phys. Rev. 92 (2) (1953) 411–415.
[41] T.R. Carver, C.P. Slichter, Experimental verification of the overhauser nuclear polarization effect, Phys. Rev. 102 (4) (1956) 975–980.
[42] I. Solomon, Relaxation processes in a system of two spins, Phys. Rev. 99 (2) (1955) 559–565.
[43] J. Jeener, B.H. Meier, P. Bachmann, R.R. Ernst, Investigation of exchange processes by two-dimensional NMR spectroscopy, J. Chem. Phys. 71 (11) (1979) 4546–4553.
[44] A. Bauder, Comment: Elucidation of cross relaxation in liquids by two-dimensional NMR spectroscopy, Mol. Phys. 100 (2002). https://doi.org/10.1080/00268970110088974.
[45] A. Kumar, R.R. Ernst, K. Wüthrich, A two-dimensional nuclear Overhauser enhancement (2D NOE) experiment for the elucidation of complete proton-proton cross-relaxation networks in biological macromolecules, Top. Catal. 95 (1) (1980) 1–6.
[46] K. Grohe, S. Patel, C. Hebrank, S. Medina, A. Klein, P. Rovó, S.K. Vasa, H. Singh, B. Vögeli, L.V. Schäfer, R. Linser, Protein Motional Details Revealed by Complementary Structural Biology Techniques, Structure 28 (9) (2020) 1024–1034.e3.
[47] J. Ilgen, J. Nowag, L. Kaltschnee, V. Schmidts, C.M. Thiele, Gradient selected pure shift EASY-ROESY techniques facilitate the quantitative measurement of 1H,1H-distance restraints in congested spectral regions, J. Magn. Reson. 324 (2021) 106900.
[48] R.W. Adams, Pure shift NMR spectroscopy, EMagRes. 3 (2014). https://doi.org/10.1002/9780470034590.emrstm1362.
[49] A. Kumar, G. Wagner, K. Wüthrich, A. Kumar, R.R. Ernst, Buildup Rates of the Nuclear Overhauser Effect Measured by Two-Dimensional Proton Magnetic Resonance Spectroscopy: Implications for Studies of Protein Conformation, J. Am. Chem. Soc. 103 (1981), https://doi.org/10.1021/ja00403a008.
[50] J. Orts, B. Vögeli, R. Riek, Relaxation matrix analysis of spin diffusion for the NMR structure calculation with eNOEs, J. Chem. Theory Comput. 8 (10) (2012) 3483–3492.
[51] D. Strotz, J. Orts, C.N. Chi, R. Riek, B. Vögeli, ENORA2 Exact NOE Analysis Program, J. Chem. Theory Comput. 13 (9) (2017) 4336–4346.
[52] D. Strotz, J. Orts, M. Minges, B. Vögeli, The experimental accuracy of the uni-directional exact NOE, J. Magn. Reson. 259 (2015) 32–46.
[53] C.N. Chi, D. Strotz, R. Riek, B. Vögeli, Extending the eNOE data set of large proteins by evaluation of NOEs with unresolved diagonals, J. Biomol. NMR. 62 (1) (2015) 63–69.
[54] C. Bergonzo, A. Grishaev, Maximizing accuracy of RNA structure in refinement against residual dipolar couplings, J. Biomol. NMR 73 (3-4) (2019) 117–139.
[55] C. Thiele, K. Petzold, J. Schleucher, EASY ROESY: Reliable cross-peak integration in adiabatic symmetrized ROESY, Chem. – A Eur. J. 15 (3) (2009) 585–588.
[56] E. Procházková, A. Kolmer, J. Ilgen, M. Schwab, L. Kaltschnee, M. Fredersdorf, V. Schmidts, R.C. Wende, P.R. Schreiner, C.M. Thiele, Uncovering Key Structural Features of an Enantioselective Peptide-Catalyzed Acylation Utilizing Advanced NMR Techniques, Angew. Chem. Int. Ed. 55 (51) (2016) 15754–15759.
[57] R. Schnieders, A.C. Wolter, C. Richter, J. Wöhnert, H. Schwalbe, B. Fürtig, Novel 13C-detected NMR Experiments for the Precise Detection of RNA Structure, Angew. Chem. Int. Ed. 58 (27) (2019) 9140–9144.
[58] R. Schnieders, S. Keyhani, H. Schwalbe, B. Fürtig, More than Proton Detection—New Avenues for NMR Spectroscopy of RNA, Chem. A Eur. J. 26 (1) (2020) 102–113.
[59] J. Kim, M. Novakovic, S. Jayanthi, A. Lupulescu, E. Kupce, J.T. Grün, K. Mertinkus, A. Oxenfarth, C. Richter, R. Schnieders, J. Wirmer-Bartoschek, H. Schwalbe, L. Frydman, 3D Heteronuclear Magnetization Transfers for the Establishment of Secondary Structures in SARS-CoV-2-Derived RNAs, J. Am. Chem. Soc. 143 (13) (2021) 4942–4948.
[60] C.F. DeLisle, H.B. Mendis, J.L. Lorieau, Super resolution NOESY spectra of proteins, J. Biomol. NMR 73 (3-4) (2019) 105–116.
[61] K. Grohe, E. Nimerovsky, H. Singh, S.K. Vasa, B. Söldner, B. Vögeli, C.M. Rienstra, R. Linser, Exact distance measurements for structure and dynamics in solid proteins by fast-magic-angle-spinning NMR, Chem. Commun. 55 (55) (2019) 7899–7902.
[62] P.J. Nichols, A. Born, M.A. Henen, D. Strotz, D.N. Jones, F. Delaglio, B. Vögeli, Reducing the measurement time of exact NOEs by non-uniform sampling, J. Biomol. NMR 74 (12) (2020) 717–739.
[63] L.H.E. Wieske, M. Erdélyi, Non-uniform sampling for NOESY? A case study on spiramycin, Magn. Reson. Chem. 59 (7) (2021) 723–737.
[64] J. Orts, B. Vögeli, R. Riek, P. Güntert, Stereospecific assignments in proteins using exact NOEs, J. Biomol. NMR 57 (3) (2013) 211–218.
[65] A. Born, M. Henen, P. Nichols, J. Wang, D. Jones, B. Vögeli, Efficient stereospecific Hβ2/3 NMR assignment strategy for mid-size proteins, Magnetochemistry 4 (2) (2018) 25.
[66] S. Grzesiek, H. Kuboniwa, A. Bax, A.P. Hinck, Multiple-Quantum Line Narrowing for Measurement of Hα—HβJ Couplings in Isotopically Enriched Proteins, J. Am. Chem. Soc. 117 (1995), https://doi.org/10.1021/ja00124a014.
[67] F. Hoffmann, M. Xue, L.V. Schäfer, F.A.A. Mulder, Narrowing the gap between experimental and computational determination of methyl group dynamics in proteins, Phys. Chem. Chem. Phys. 20 (38) (2018) 24577–24590.
[68] F. Hoffmann, F.A.A. Mulder, L.V. Schäfer, Accurate Methyl Group Dynamics in Protein Simulations with AMBER Force Fields, J. Phys. Chem. B 122 (19) (2018) 5038–5048.
[69] I. Kuprov, L.C. Morris, J.N. Glushka, J.H. Prestegard, Using molecular dynamics trajectories to predict nuclear spin relaxation behaviour in large spin systems, J. Magn. Reson. 323 (2021) 106891.
[70] F. Vasile, G. Tiana, Determination of Structural Ensembles of Flexible Molecules in Solution from NMR Data Undergoing Spin Diffusion, J. Chem. Inf. Model. 59 (6) (2019) 2973–2979.
[71] N. Sibille, A. Pardi, J.P. Simorre, M. Blackledge, Refinement of local and long-range structural order in theophylline-binding RNA using 13C–1H residual dipolar couplings and restrained molecular dynamics, J. Am. Chem. Soc. 123 (2001), https://doi.org/10.1021/ja011646+.
[72] O. Mauffret, G. Tevanian, S. Fermandjian, Residual dipolar coupling constants and strucuture determination of large DNA duplexes, J. Biomol. NMR 24 (2002), https://doi.org/10.1023/A:1021645131882.
[73] Y. Shen, A.d. Bax, Protein backbone and sidechain torsion angles predicted from NMR chemical shifts using artificial neural networks, J. Biomol. NMR 56 (3) (2013) 227–241.
[74] L. Salmon, G.M. Giambaşu, E.N. Nikolova, K. Petzold, A. Bhattacharya, D.A. Case, H.M. Al-Hashimi, Modulating RNA Alignment Using Directional Dynamic Kinks: Application in Determining an Atomic-Resolution Ensemble for a Hairpin using NMR Residual Dipolar Couplings, J. Am. Chem. Soc. 137 (40) (2015) 12954–12965.
[75] S. Nozinovic, B. Fürtig, H.R.A. Jonker, C. Richter, H. Schwalbe, High-resolution NMR structure of an RNA model system: The 14-mer cUUCGg tetraloop hairpin RNA, Nucl. Acids Res. 38 (2) (2010) 683–694.
[76] S. Bottaro, P.J. Nichols, B. Vögeli, M. Parrinello, K. Lindorff-Larsen, Integrating NMR and simulations reveals motions in the UUCG tetraloop, Nucl. Acids Res. 48 (11) (2020) 5839–5848.
[77] A. Born, J. Soetbeer, F. Breitgoff, M.A. Henen, N. Sgourakis, Y. Polyhach, P. J. Nichols, D. Strotz, G. Jeschke, B. Vögeli, Reconstruction of Coupled Intra- And Interdomain Protein Motion from Nuclear and Electron Magnetic Resonance, J. Am. Chem. Soc. 143 (39) (2021) 16055–16067.
[78] E. Bayer, S. Goettsch, J.W. Mueller, B. Griewel, E. Guiberman, L.M. Mayr, P. Bayer, Structural analysis of the mitotic regulator hPin1 in solution: Insights into domain architecture and substrate binding, J. Biol. Chem. 278 (28) (2003) 26183–26193.
[79] B. Vögeli, T.F. Segawa, D. Leitz, A. Sobol, A. Choutko, D. Trzesniak, W. van Gunsteren, R. Riek, Exact distances and internal dynamics of perdeuterated ubiquitin from NOE buildups, J. Am. Chem. Soc. 131 (47) (2009) 17215–17225.
[80] C. Kolloff, A. Mazur, J.K. Marzinek, P.J. Bond, S. Olsson, S. Hiller, Motional clustering in supra- τ c conformational exchange influences NOE cross-relaxation rate, J. Magn. Reson. 338 (2022), https://doi.org/10.1016/j.jmr.2022.107196.
[81] P. Güntert, A B-factor for NOEs? J. Magn. Reson. 338 (2022) 107189.
[82] D.M. LeMaster, L.E. Kay, A.T. Brünger, J.H. Prestegard, Protein dynamics and distance determination by NOE measurements, FEBS Lett. 236 (1) (1988) 71–76.
[83] C.A. Smith, A. Mazur, A.K. Rout, S. Becker, D. Lee, B.L. de Groot, C. Griesinger, Enhancing NMR derived ensembles with kinetics on multiple timescales, J. Biomol. NMR. 74 (1) (2020) 27–43.
[84] J. Borggräfe, J. Victor, H. Rosenbach, A. Viegas, C.G.W. Gertzen, C. Wuebben, H. Kovacs, M. Gopalswamy, D. Riesner, G. Steger, O. Schiemann, H. Gohlke, I. Span, M. Etzkorn, Time-resolved structural analysis of an RNA-cleaving DNA catalyst, Nature 601 (2022) 144–149, https://doi.org/10.1038/s41586-021-04225-4.
[85] K.P. Lu, Prolyl isomerase Pin1 as a molecular target for cancer diagnostics and therapeutics, Cancer Cell. 4 (3) (2003) 175–180.
[86] S.L. Ma, L. Pastorino, X.Z. Zhou, K.P. Lu, Prolyl isomerase Pin1 promotes amyloid precursor protein (APP) turnover by inhibiting glycogen synthase kinase-3β (GSK3β) activity: Novel mechanism for Pin1 to protect against alzheimer disease, J. Biol. Chem. 287 (10) (2012) 6969–6973.

[87] Y.-C. Liou, X.Z. Zhou, K.P. Lu, Prolyl isomerase Pin1 as a molecular switch to determine the fate of phosphoproteins, Trends Biochem. Sci. 36 (10) (2011) 501–514.
[88] J.W. Peng, Investigating dynamic interdomain allostery in Pin1, Biophys. Rev. 7 (2) (2015) 239–249.
[89] D. Strotz, J. Orts, H. Kadavath, M. Friedmann, D. Ghosh, S. Olsson, C.N. Chi, A. Pokharna, P. Güntert, B. Vögeli, R. Riek, Protein Allostery at Atomic Resolution, Angew. Chem. Int. Ed. 59 (49) (2020) 22132–22139.
[90] R. Ranganathan, K.P. Lu, T. Hunter, J.P. Noel, Structural and functional analysis of the mitotic rotamase Pin1 suggests substrate recognition is phosphorylation dependent, Cell 89 (6) (1997) 875–886.
[91] B. Vogeli, A. Born, J. Soetbeer, M. Henen, F. Breitgoff, Y. Polyhach, G. Jeschke, Ligand-specific conformational change drives interdomain allostery in Pin1, Nat. Commun. 13 (2022), https://doi.org/10.1038/s41467-022-32340-x.